ACS OMEGA

Open Access

http://pubs.acs.org/journal/acsodf

Article

Performance Prediction and Heating Parameter Optimization of Organic-Rich Shale In Situ Conversion Based on Numerical Simulation and Artificial Intelligence Algorithms

Yaqian Liu, Chuanjin Yao,* Baishuo Liu, Yangyang Xuan, and Xinge Du

Cite This: *ACS Omega* 2024, 9, 15511−15526

Read Online

ACCESS | Metrics & More | Article Recommendations

ABSTRACT: In situ conversion technology is a green and effective way to realize the development of organic-rich shale. Supercritical CO_2 can be used as a good heating medium for shale in situ conversion. Numerical simulation is an important means to explore the shale in situ conversion process, but it requires a lot of time and computational cost for in situ conversion simulation under different working conditions. Therefore, a computational framework for rapid prediction of shale in situ conversion development performance and heating parameter optimization is proposed by coupling artificial neural network (ANN) and particle swarm optimization (PSO). The results indicated that kerogen pyrolysis and hydrocarbon product release mainly occurred within 2 years of shale in situ conversion. The production curves of pyrolysis hydrocarbon obviously slowed after in situ conversion for 2 years. The database was constructed by a large number of in situ conversion simulations, and Pearson correlation analysis and the random forest method were adopted to obtain seven main controlling factors affecting reservoir temperature and hydrocarbon production. The determination coefficient of the obtained ANN-based prediction models is higher than 97%, and the mean square error (MSE) is lower than 0.3%. The basic reservoir case can choose to inject 350−450 °C supercritical CO_2 (Sc-CO_2) fluid with a rate of 600 m^3/day to obtain a more promising development effect. The heating parameter optimization for three typical reservoir cases using PSO was performed, and reasonable injection temperature and injection rate were obtained. It realized accurate development prediction and rapid heating parameter optimization, which helps the effective application of shale in situ conversion development design.

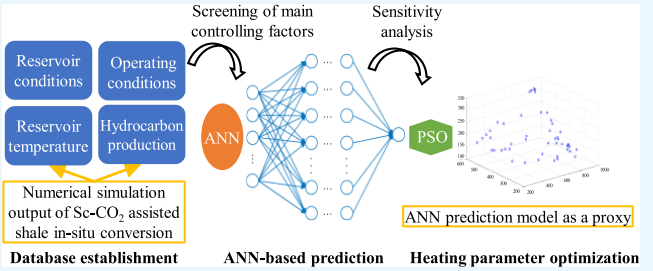

1. INTRODUCTION

With the success of the shale oil and gas revolution in the United States, the exploration and development of shale resources in China have increased significantly.[1] The continental shale resource is huge in China, so it is an important energy replacement field, in which medium-low-maturity shale oil occupies the main position with (700−900) × 10^8 of technically recoverable resources.[1] The medium- to low-maturity shale contains unconverted kerogen and undischarged liquid hydrocarbons. The hydrocarbon generation potential is huge, but the effective development and utilization of medium-low-maturity shale oil is a major challenge.[3] At present, the development technology of medium-low-maturity shale oil includes ground retorting and in situ conversion technology.[4−6] The retorting technology is suitable for shallow organic-rich shale, and it will produce a large amount of polluting gases, which is contrary to the concept of environmentally friendly development proposed by China.[7,8] In contrast, in situ conversion technology is considered to be an efficient, green, and feasible way. With the application and promotion of Shell's ICP technology, research on electric heating in situ conversion has increased in China.[9,10] However, due to low permeability and poor thermal conductivity of shale, the heating efficiency of electric heating is low and the heating speed is slow.[6] On this basis, convective heating attracts more attention, which is attributed to the pressurization effect, the increasing formation heating rate, the gas driving mechanism, and the enhanced hydrocarbon production.[11−15] Supercritical CO_2 has a high diffusion coefficient, low viscosity and surface tension, and the ability of strong permeability and solubility.[16,17] At the same time, it can also achieve a certain degree of carbon sequestration effect, which is consistent with the strategic goals of the carbon peak and carbon neutralization. Therefore, supercritical CO_2 can be used as a heating medium for shale in situ conversion. Mozaffari et

Received: January 10, 2024
Revised: March 7, 2024
Accepted: March 12, 2024
Published: March 20, 2024

https://doi.org/10.1021/acsomega.4c00323
ACS Omega 2024, 9, 15511−15526

al. evaluated that, compared with the nitrogen environment, CO_2 was conducive to the generation of more liquid products, which was promising in increasing the yield of pyrolysis oil.[18] Allawzi et al. confirmed a rapid extraction ability of supercritical CO_2 for oil shale, which presented a reference method for extracting shale oil from oil shale.[14] Zhao et al. researched Huadian oil shale pyrolysis behavior under supercritical CO_2, which concluded that supercritical CO_2 could effectively extract organic matter from shale.[19] Heating temperature, residence time, and environmental pressure affected the composition and recovery of the hydrocarbon products.

Numerical simulation is an important means to investigate the in situ conversion performance of organic-rich shale. It can realize fluid convection heating, in situ conversion of organic matter, and hydrocarbon production at the field scale, which can provide valuable references for in situ conversion under actual working conditions.[20−22] This is difficult to achieve on an experimental scale. Zhu et al. used CMG commercial software to simulate the dynamic evolution during nitrogen-assisted shale in situ conversion and analyzed the response of oil recovery to injection temperature, total organic carbon content, and closed area.[23] Youtsos et al. quantitatively compared the migration law of the thermal front and reaction front of shale in situ conversion by conduction heating and convection heating using numerical calculation.[24] Pei et al. used the CMG-STARS module to compare the production and energy efficiency of in situ conversion by conduction and nitrogen-assisted heating, which found that convective heating could greatly improve heat transfer efficiency and oil recovery.[13] Zhao et al. conducted a numerical simulation of in situ conversion for low mature shale and realized evolution of temperature field, seepage field, and stress field in this process based on theoretical analysis.[25] Wang et al. studied the effects of heating temperature, heating mode, and initial kerogen concentration on production results by numerical simulation for medium to low maturity shale reservoirs in situ conversion.[26] However, on the one hand, there are few numerical simulation studies on supercritical CO_2-assisted in situ conversion. On the other hand, the production effect and the optimal heating parameters of in situ conversion depend upon its physical characteristics. For organic-rich shale with different geological conditions and reservoir characteristics, different development schemes may be adopted to achieve effective in situ conversion, which requires corresponding numerical simulation models to run in turn. This process requires a large amount of time and computational costs.

On the contrary, the artificial intelligence method helps to greatly reduce the simulation time and this method is widely used in hydrocarbon production prediction and development parameter optimization in the petroleum industry.[27−32] Chen et al. applied the ANN to predict the diffusion coefficients of CO_2 in porous media.[33] Al-Khafaji et al. used machine learning methods to achieve rapid prediction for the minimum miscible pressure of CO_2, showing superior accuracy and adaptability than traditional methods.[34] Kalam et al. found that the ANN is superior to the adaptive neural fuzzy inference system and support vector regression in the prediction accuracy and calculation efficiency of water flooding recovery.[35] You et al. combined machine learning and PSO optimization algorithms to comprehensively optimize the oil recovery-CO_2 storage effect.[36] However, artificial intelligence methods are rarely used to predict and optimize shale in situ conversion performance. Therefore, this paper established the numerical simulation model of supercritical CO_2-assisted shale in situ conversion based on the reservoir characteristics of organic-rich shale in China, and it quantitatively analyzed the development performances. Furthermore, the ANN method was used to quickly predict the reservoir temperature and hydrocarbon production performance of supercritical CO_2-assisted shale in situ conversion. The heating parameter design optimization is carried out using the established ANN prediction model as a proxy and PSO algorithm. The prediction and optimization framework proposed in this paper can provide some theoretical and technical reference for the development design of organic-rich shale in situ conversion.

2. NUMERICAL SIMULATION

2.1. Reservoir Simulation Model Description. The in situ conversion process is a complex multifield coupling process. The temperature and pressure of the shale reservoirs increased because of convection heating. The concentrations of the pseudo-components were dynamically changed by kinetic reactions, phase transport, and fluid seepage in porous media. The shale porosity and permeability evolved along with kerogen pyrolysis, phase transitions, thermal expansion of the rock and fluid, and fluid transport. At the same time, cracks or fractures may be generated due to thermal effects. Therefore, a dual-permeability model was established to characterize fluid seepage in the reservoir matrix and fracture by using the CMG-STARS module. The model was discretized into Cartesian grid blocks with a uniform grid size of 0.7 × 0.4 m. The level of meshing here was determined to be appropriate by multiple simulation tests. The reservoir depth was 1500 m. The initial formation temperature and pressure were 70 °C and 18.1 MPa, respectively. The porosities of the matrix and fracture were 4 and 15%, respectively. The permeabilities of the matrix and fracture were 0.1×10^{-3} μm^2 and 100×10^{-3} μm^2, respectively. The fracture spacing was set to 3 m. Solid kerogen with a concentration of 15,500 mol/m^3 was evenly distributed in the pores of the shale reservoir. Fan et al. proved that the hexagonal well pattern could obtain faster hydrocarbon productions and higher recovery.[37] It is more practical to study the in situ conversion of hexagonal well patterns. Therefore, a numerical simulation model of supercritical CO_2-assisted shale in situ conversion was established, referring to the hexagonal well pattern in the Mahogany project.[38] Due to the pattern symmetry and the time cost of running a large number of numerical simulation models, only one-sixth of the hexagonal well pattern was studied and other grids were set to invalid grids.[13] Finally, the total hydrocarbon production for the hexagonal well pattern could be obtained by multiplying the oil and gas production data of the simulation model by 6.[37] In this paper, two heaters and one producer were set up in the simulation model. All layers of the well were penetrated. The temperature of supercritical CO_2 injection was 400 °C, and the injection rate was 800 m^3/day. The simulation model of Sc-CO_2-assisted shale in situ conversion is shown in Figure 1.

Most of the existing simulation studies do not consider the heat loss caused by the overburden and underburden bedrock, which is important for the large-scale application of shale in situ conversion.[37] Based on the basic physical properties of shale and bedrock in the published data, the volumetric heat capacity and thermal conductivity of the shale were set to be 5.0×10^6 J/(m^3·°C) and 216,000 J/(m·day·°C), respectively. The volumetric heat capacity and thermal conductivity of the

https://doi.org/10.1021/acsomega.4c00323
ACS Omega 2024, 9, 15511−15526

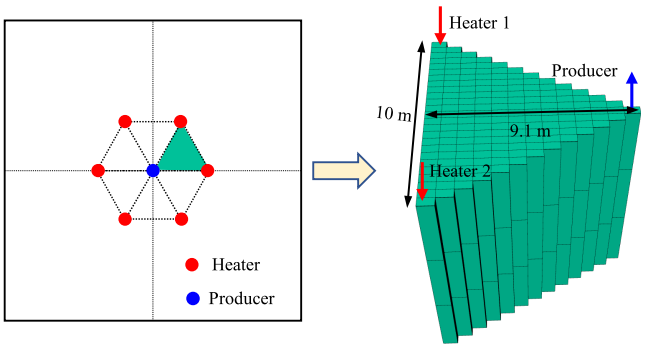

Figure 1. Numerical simulation model of Sc-CO_2-assisted shale in situ conversion.

overburden and underburden bedrock were 3.24×10^6 J/(m^3·°C) and 86400 J/(m·day·°C), respectively.[25,39] Then, heat loss during the in situ conversion was considered. The organic-rich shale reservoir included rocks and pores, and the pores were filled with organic kerogen and fluid. As supercritical CO_2 was injected, it accompanied organic matter pyrolysis, inorganic mineral transformation, and rock thermal expansion. These three effects mainly influence the porosity and permeability. The thermal expansion coefficient of rock was set to 5×10^{-6} °C^{-1}. The influence of inorganic mineral transformation on shale porosity and permeability is less than that of organic matter pyrolysis.[40] Moreover, from the thermogravimetric curve, the reservoir temperature involved in the actual in situ conversion is mainly within the range of organic matter pyrolysis, which is not enough to activate the reaction of inorganic minerals.[24] Therefore, the changes in the shale porosity and permeability caused by the organic matter pyrolysis reaction were considered. The Kozeny-Carman model is used to characterize the permeability as a function of porosity, which is calculated by eq 1.

$$K = \frac{2C_{on}K_o\phi}{\phi_o} \times \frac{1-\phi_o}{1-\phi} \tag{1}$$

where K and ϕ are the permeability and porosity after deformation, respectively. K_0 and ϕ_o are the initial permeability and porosity, respectively. C_{on} is a constant set to 2 here.

The oil−water and gas−liquid relative permeability curves of the matrix in this article are shown in Figure 2, and the relative permeability curve of the fracture is X-shaped.

2.2. Fluids and Flow Models. At present, many kinetic models of organic matter pyrolysis have been proposed,[41−44] among which the most widely used are the Braun and Burnham model (BB model) and the Wellington model (W model).[43,44] Lee et al. compared the application effects of these two kinetic models and found that the BB model could produce more oil and gas and the pyrolysis reaction was more intense.[45] In this paper, the W model adjusted in our previous research work was adopted, which mainly included three alternating reactions of kerogen pyrolysis, heavy oil cracking, and light oil cracking, as shown in Table 1.[46] Referring to the pyrolysis experimental data given by Braun and Burnham,[43,47] it involves a variety of oil and gas components. According to the principle of similar component properties, oil-1 to oil-6 were lumped and defined as IC_{13}, oil-7 to oil-11 were lumped into IC_{37}, and CH_4 and CH_x were lumped into IC_2. Kerogen, prechar, IC_{37}, IC_{13}, and IC_2 were used to represent kerogen, solid residue, heavy oil, light oil, and hydrocarbon gas, respectively. This practice has been verified for its rationality.[37,45,46] The detailed properties of each pseudocomponent are presented, as shown in Table 2. The initial oil content is set at 5% in the simulation, and the initial oil is set as the IC_{37} material.[25]

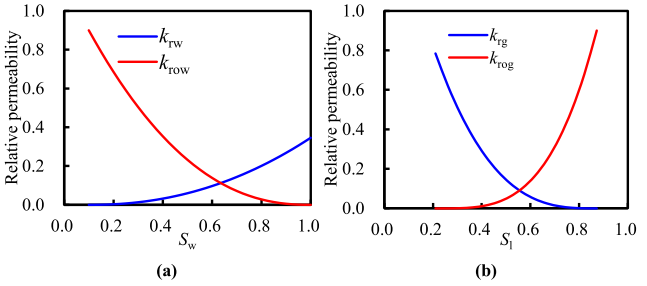

Figure 2. Curves of (a) oil−water relative permeability and (b) gas−liquid relative permeability.

The oleic phase viscosity at different temperatures is calculated using eq 2, and the mixture viscosity is determined by the molar fractions of the pseudo-components according to the linear mixing rule.[48] K values for gas−liquid equilibrium are calculated by using eq 3. The density of the oil and gas phases changes with reservoir temperature and pressure. The pyrolysis reaction equation, reaction frequency factor, activation energy, and reaction enthalpy are used as the input parameters of the kinetic simulation.

$$\mathrm{VISC} = \mathrm{AVISC} \times e^{\mathrm{BVISC}/T+273.15} \tag{2}$$

where VISC is the liquid equivalent viscosity, in mPa·s. AVISC and BVISC are the corresponding coefficients.

$$K_{value} = \frac{KV_1}{P} \times e^{KV_4/T-KV_5} \tag{3}$$

where K_{value} is the K value at a certain temperature and pressure. KV_1, KV_4, and KV_5 are corresponding coefficients. P is the pressure, in kPa. T is the temperature, in °C.

3. METHODOLOGY

Combined with numerical simulation technology and machine learning, the performance prediction and parameter optimization models of shale in situ conversion via Sc-CO_2 injection are established. The specific workflow includes the following steps: (a) Detailed data on shale reservoir characteristics and development operating are collected, and a numerical simulation model of in situ conversion is established via Sc-CO_2 injection. (b) The general parameters that affect the shale in situ conversion performance are selected, and the sample database is generated and optimized. (c) The prediction model of Sc-CO_2-assisted shale in situ conversion is constructed and evaluated based on ANN methodology. (d) The heating parameters are optimized using the PSO algorithm with the ANN prediction model as a proxy.

3.1. Database Establishment. The factors affecting organic-rich shale in situ conversion via fluid heating usually include reservoir conditions and production operating conditions. There are 12 influencing factors considered, including reservoir depth, thickness, initial reservoir temperature and pressure, matrix permeability, natural fracture permeability, porosity, natural fracture spacing, initial kerogen concentration, Sc-CO_2 injection rate, injection temperature, and production pressure.[21,23,24,37] Zhao et al. evaluated that

https://doi.org/10.1021/acsomega.4c00323
ACS Omega 2024, 9, 15511−15526

Table 1. Characterization Model of Organic Matter Pyrolysis Reaction

reactions	stoichiometry	frequency factor (s^{-1})	reaction enthalpy ($kJ·mol^{-1}$)	activation energy ($kJ·mol^{-1}$)
kerogen decomposition	kerogen →0.02691H_2O + 0.005888IC_{37} + 0.0178IC_{13} + 0.04175IC_2 + 0.00541CO_2 + 0.5827prechar	3.74×10^{12}	335.00	161.600
cracking of heavy oil	IC_{37} → 0.6463IC_{13} + 4.465IC_2 + 17.497prechar	2.65×10^{20}	46.50	206.034
cracking of light oil	IC_{13} → 1.023IC_2 + 10.904prechar	3.82×10^{20}	46.50	219.328

Table 2. Detailed Properties of Pseudo-components

properties	IC_{37}	IC_{13}	IC_2	CO_2	water	kerogen	prechar
molecular weight ($kg·mol^{-1}$)	0.46583	0.16952	0.03007	0.04401	0.01802	0.1515	0.1272
critical temperature (°C)	689.133	442.211	15.5944	31.05	374		
critical pressure (kPa)	1470.03	2405.03	4609.01	7376	22106		
KV_1 (kPa)	1.8929×10^6	1.3271×10^6	8.4644×10^5	8.6212×10^8	1.1860×10^7		
KV_4 (°C)	−4680.46	−3774.56	−1511.42	−3103.39	−3816.44		
KV_5 (°C)	−132.05	−181.84	−255.99	−272.99	−227.02		
AVISC (mPa·s)	0.0345	0.0656	0.0818	0.1156	0.0047		
BVISC (°C)	1082.29	534.71	156.6	182.63	1515.7		

shale with a depth of 300−3000 m is suitable for in situ conversion technology.[1] Besides, the survey found that the continental shale reservoir in China is mostly at depths of 1000−3000 m.[1,2,49,50] Therefore, the in situ conversion of shale in this depth range was predicted. The formation pressure gradient is selected as 1.2 MPa/hm, and the geothermal gradient is 3.0 °C/hm.[1,49] According to the shale depth, the initial temperature and pressure can be determined by the geothermal and pressure gradient, respectively. It is worth mentioning that the shale reservoir temperature and pressure calculated meet the supercritical state of CO_2 (7.38 MPa, 31.26 °C). The temperature and pressure in the reservoir increase linearly with the depth. The range of the influence factors is determined by referring to the existing public data, as shown in Table 3.

Two evaluation responses of average reservoir temperature and cumulative hydrocarbon production are selected to achieve the performance prediction of shale in situ conversion via fluid heating. The hydrocarbon gas of 975 sm^3 is defined as the unit oil equivalent.[13] The cumulative hydrocarbon production is determined by the cumulative oil equivalents from oil and hydrocarbon gas generated. The Latin hypercube sampling method, which has a distribution function more accurately estimated than Monte Carlo, was used,[51] and then 430 simulation cases were generated with normal distribution probability in the input space of the selected parameters. Based on the established simulation model of shale in situ conversion by Sc-CO_2 injection, all simulation schemes were run. The simulation output of shale in situ conversion for 1500 days was counted to construct the basic sample database composed of the influencing factors and the corresponding evaluation responses.

3.2. Database Optimization. Many factors considered in this paper have a great or small influence on the average temperature and hydrocarbon production. It is necessary to capture which variables have a significant effect on target responses. This makes the neural network model respect the physics and chemistry of in situ conversion and have a good prediction performance.[29] Therefore, Pearson correlation analysis and random forest analysis are used to screen the main controlling factors to obtain an optimized database.

Table 3. Influencing Factors and Ranges of Shale In-Situ Conversion via Sc-CO_2 Injection

input parameters	units	lower limit	upper limit	comments
depth (D)	m	1000	3000	normal distribution
thickness (h)	m	3	180	normal distribution
original reservoir pressure (P_o)	MPa	12.1	36.1	P = 0.1+ 0.012D
original reservoir temperature (T_o)	°C	55	115	T = 25 + 0.03D
original permeability for matrix (k_{om})	10^{-3} μm^2	0.005	0.15	normal distribution
original porosity for matrix (ϕ_{om})	%	2.0	10.0	normal distribution
original permeability for natural fracture (k_{of})	10^{-3} μm^2	10	100	normal distribution
natural fracture spacing (S)	m	0.1	3	normal distribution
concentration of kerogen in the pore (C)	mol/m^3	2000	20000	normal distribution
Sc-CO2 injection rate (R_{inj})	m^3/day	100	1000	normal distribution
injection temperature of Sc-CO_2 (T_{inj})	°C	300	600	normal distribution
production pressure difference (ΔP)	kPa	2000	6000	normal distribution

Pearson correlation analysis is widely adopted to measure the linear correlation relation between features through correlation coefficients so that redundant features can be eliminated.[33,52] There may be a nonlinear correlation between the factors and responses. Therefore, Pearson correlation analysis is used only to calculate the correlation degree between the influencing factors. When the correlation coefficient between two variables is higher than 0.8, there is a strong linear correlation between the two, and one of the variables should be eliminated.[53,54] The Pearson correlation coefficient can be calculated using eq 4.

https://doi.org/10.1021/acsomega.4c00323
ACS Omega 2024, 9, 15511−15526

$$r = \frac{\sum_{t=1}^{q}\left(a_t - \frac{1}{q}\sum_{t=1}^{q} a_t\right)\left(b_t - \frac{1}{q}\sum_{t=1}^{q} b_t\right)}{\sqrt{\sum_{t=1}^{q}\left(a_t - \frac{1}{q}\sum_{t=1}^{q} a_t\right)^2}\sqrt{\sum_{t=1}^{q}\left(b_t - \frac{1}{q}\sum_{t=1}^{q} b_t\right)^2}} \quad (4)$$

where r is the correlation coefficient of data pairs $(a_t b_t)(t = 1,2,\cdots,q)$. The correlation coefficient r ranges from −1 to 1.

Moreover, random forest is used to evaluate the contribution of features to the target response to further screen the key factors of shale in situ conversion. Random forest is an ensemble learning algorithm. By combining multiple decision trees together, the prediction results of a random forest are generated according to the voting results of all trees.[55] The algorithm realizes the randomness of ensemble learning through the two characteristics of random sampling to construct the training set and the sampling method with replacement. It ensures the high accuracy and generalization performance of the random forest method. Therefore, the random forest algorithm was used to obtain variation importance measures (VIM) to rank the contribution of each variable by the Gini index.[56,57]

3.3. ANN-Based Prediction Model. An artificial neural network is composed of huge amounts of neurons, which can realize nonlinear mapping of the whole network from input to output space.[58−60] It is a data-driven adaptive technology with the ability to organize and learn.[33] It is one of the most widely used prediction techniques. The neural network consists of an input layer, a hidden layer, and an output layer. The number of neurons in the input layer and the output layer is determined by the influencing factors and target parameters. There can be multiple hidden layers, and each layer can have different numbers of neurons. The input signal is transmitted through a weighted connection; the total input signal received by the neuron is compared with the threshold; and the output is generated by the activation function. The number of hidden layers and hidden layer neurons, the activation function, the training function, and the learning rate are the variables of neural network architecture optimization. The optimal neural network hyperparameters can be obtained through multiple neural network trainings and predictions under different ANN architectures. In this paper, a back-propagation (BP) neural network, which is a multilayer feedforward neural network trained by error back-propagation, is used to update weights and thresholds to minimize the difference between network output and expected output.[33,60,61] The input data here are the main controlling factors after screening, and the model outputs are the average reservoir temperature and cumulative hydrocarbon production. The application of the BP neural network includes the following steps: The model training set and testing set are divided and data normalized using eq 5.[29,33] The neural network structure and hyperparameters are given. (c) The connection weights and thresholds between the input layer, hidden layer, and output layer neurons are initialized. (d) The output of the hidden layer and output layer is calculated to determine the network prediction error using eq 6. (e) Based on the model calculation error, the connection weight and threshold are updated using eq 7. (f) Whether the iteration ends is determined. If not, step (d) is repeated.[33]

$$X = \frac{x - x_{\min}}{x_{\max} - x_{\min}} \quad (5)$$

where x is the original data. X is the corresponding value after normalization. $x_{\max}$ and $x_{\min}$ are the maximum and minimum values of the original data set.

$$H_j = f_1\left(\sum_{i=1}^{n} \upsilon_{ij} X_i - \theta_j\right)$$

$$O_k = f_2\left(\sum_{j=1}^{l} H_j \omega_{jk} - \gamma_k\right)$$

$$e_k = Y_k - O_k \quad (6)$$

$$\upsilon_{ij} = \upsilon_{ij} + \eta H_j(1 + H_j)X(i)\sum_{k=1}^{m} \omega_{jk} e_{jk}$$

$$\omega_{jk} = \omega_{jk} + \eta H_j e_k$$

$$\theta_j = \theta_j + \eta H_j(1 - H_j)\sum_{k=1}^{m} \omega_{jk} e_k$$

$$\gamma_k = \gamma_k + e_k \quad (7)$$

where H is the hidden layer output, O is the output layer output, and e is the network calculation error. n, l, and m are the number of nodes in the input layer, hidden layer, and output layer, respectively. υ_{ij} is the connection weight between the ith neuron in the input layer and the jth neuron in the hidden layer, and ω_{jk} is the connection weight between the jth neuron in the hidden layer and the kth neuron in the output layer. θ and γ are the thresholds of the hidden layer and the output layer, respectively. f_1 and f_2 are the excitation functions of the hidden layer and output layer, respectively. Y is the expected output. η is the network learning rate.

3.4. Heating Parameter Design Optimization. The design of heating parameters is optimized by adopting the PSO algorithm based on the established ANN prediction model as a proxy. PSO is a random cooperative optimization algorithm, which is proposed based on simulating the population behavior of birds.[62,63] Particles are equivalent to individuals, and a particle swarm is a population. During finding the optimal solution in the domain space, the behavior of the particle is controlled by the two parameters of the position and velocity.[64] The generation is continuously updated by tracking individual and global solutions. The velocity and position of the particles are updated using eqs 8 and 9, respectively.[63,64]

$$v_{i+1} = \kappa^* v_i + c_1 \mathrm{rand}_1(p_i - \chi_i) + c_2 \mathrm{rand}_2(g_i - \chi_i) \quad (8)$$

$$\chi_{i+1} = \chi_i + v_{i+1} \quad (9)$$

where κ is the inertial factor, c_1 is the learning rate representing a cognitive term, and c_2 is the learning rate representing a social component. rand_1 and rand_2 are random factors between 0 and 1. p_i is the individual optimal position searched by a single particle up to the ith update, and g_i is the global optimal position. v_i and χ_i are the particle velocity and position at the ith update, respectively. v_{i+1} and χ_{i+1} are the particle velocity and position at the $(i+1)$th update, respectively. The trajectory of particles in the domain space is defined by inertia factor, cognitive term, and social component.[62,65]

https://doi.org/10.1021/acsomega.4c00323
ACS Omega 2024, 9, 15511−15526

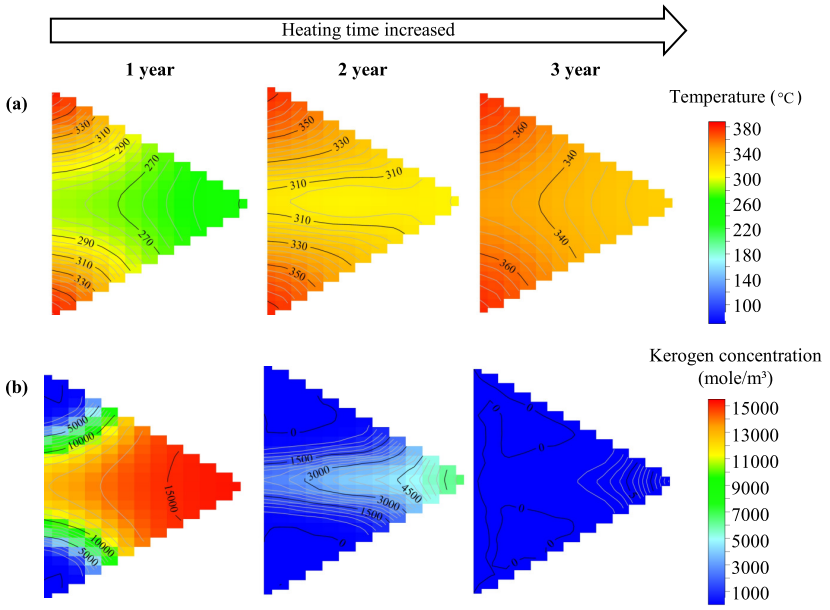

Figure 3. Field diagram of shale in situ conversion by Sc-CO_2 injection for (a) temperature field and (b) kerogen concentration field.

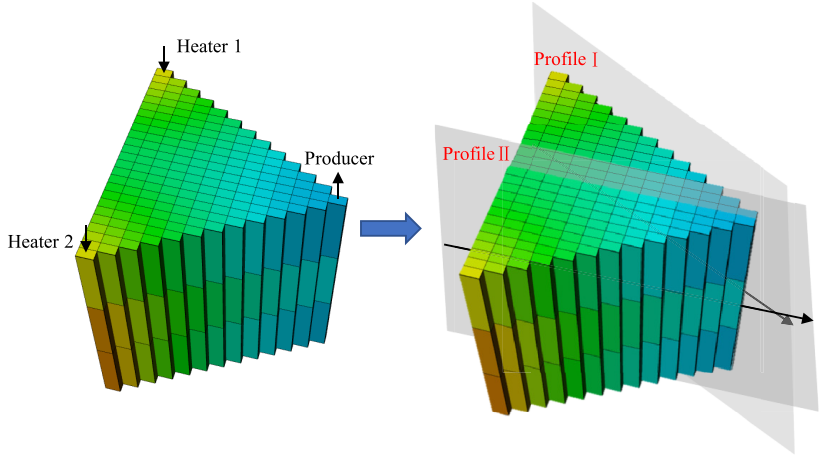

Figure 4. Diagram of quantitative evaluation for organic-rich shale in situ conversion performance.

4. RESULTS AND DISCUSSION

4.1. Performance of Shale In Situ Conversion. With the continuous injection of supercritical CO_2, the reservoir temperature rose. In order to quantitatively analyze the heating process, the temperature field diagram and kerogen concentration field diagram from the output simulated by CMG-STARS were further drawn by Sufer software. The temperature field and kerogen concentration field of the middle layer after heating for 1, 2, and 3 years are shown in Figure 3. The area near the heater was first heated by the thermal fluid, and its temperature was higher than that of the reservoir deep. The cracking of organic matter is dependent on the reservoir temperature. Therefore, the kerogen near the heater was first pyrolyzed, causing a lower concentration. The high diffusivity and thermal conductivity of Sc-CO_2 make the convective heating in shale reservoirs very fast. Wang et al. pointed out that about 300 °C is the starting temperature of kerogen cracking.[26] When shale in situ conversion was conducted for 1 year, the temperature of 29.6% of the shale grid cells reached 300 °C. After heating for 2 years, the temperature of all grids was higher than 300 °C and an average of 82.5% of reservoir kerogen was cracked. After Sc-CO_2 injection for 3 years, the kerogen in the middle layer of the simulation model was basically completely pyrolyzed. It can be concluded from Figure 3 that the front of the kerogen pyrolysis completion zone is synchronized with a temperature front of about 340 °C.

In order to quantitatively analyze the hydrocarbon product distribution characteristics during in situ conversion, the connection plane between heater 1 and the producer was defined as profile I and the plane between the producer and the middle grid of two heaters was profile II, as shown in Figure 4. The content changes of light oil, heavy oil, and hydrocarbon gas in the middle layer grid of the two profiles were mainly analyzed. For profile I, the heater position was defined as the origin, and the producer position was the dimensionless distance of 1. For profile II, the middle position of the two heaters was the origin while the producer was the dimensionless distance of 1.

After Sc-CO_2 was injected into the shale reservoir, the shale reservoir was heated rapidly due to heat transfer and the organic matter was cracked. The generated pyrolysis oil and gas migrated to the producer under the concentration gradient

https://doi.org/10.1021/acsomega.4c00323
ACS Omega 2024, 9, 15511−15526

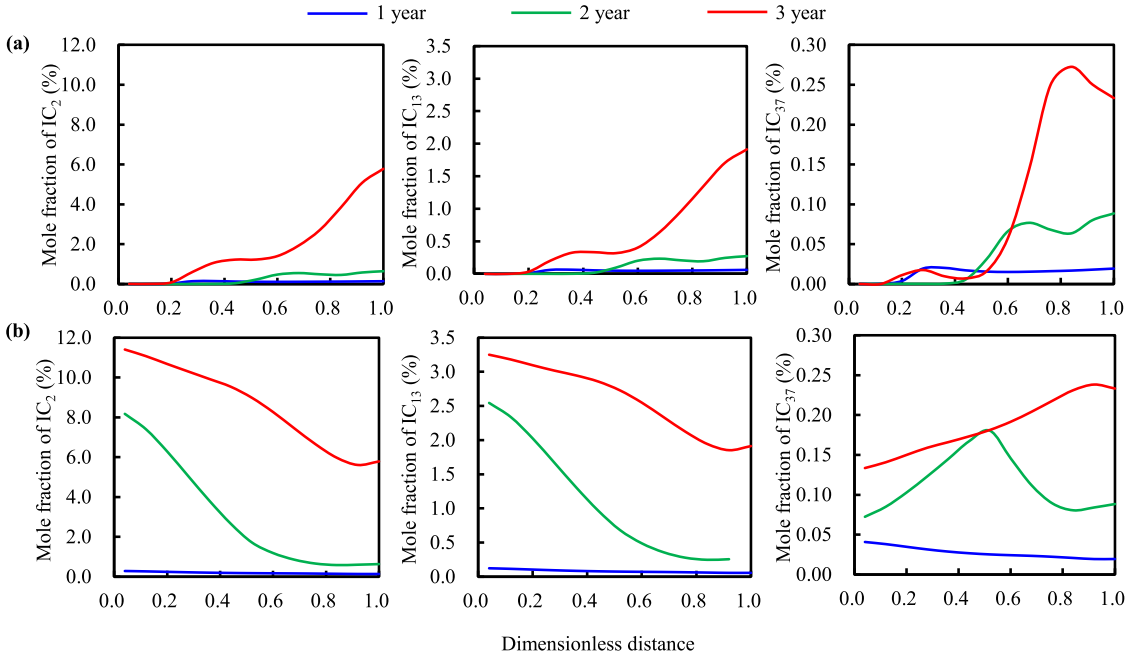

Figure 5. Distribution characteristics of pyrolysis hydrocarbon products for (a) profile I and (b) profile II.

and pressure gradient. The content changes of light oil, heavy oil, and hydrocarbon gas in profiles I and II under different heating times were plotted, as shown in Figure 5. The pyrolysis oil and gas were more pronounced with the increase in in situ conversion time. For the content change of oil and gas products in profile I, due to the cracking of kerogen near the heater, the porosity and permeability of the reservoir increased, which was conducive to the seepage of oil and gas products. The oil and gas were continuously displaced by Sc-CO_2. Finally, there is almost no pyrolysis oil and gas in the area within the dimensionless distance of 0.2 when the shale in situ conversion was carried out for 1 year while the content of hydrocarbon gas, light oil, and heavy oil in profile II was higher than that in profile I, as shown in the blue line in Figure 5a,b. The content of hydrocarbon gas, light oil, and heavy oil in the grid cells within the dimensionless distance of 0.44 for profile I was almost 0 after shale in situ conversion for 2 years.

At in situ conversion for 1 year, the kerogen near the two heaters was mainly cracked. As Sc-CO_2 was injected, the pyrolysis completion zone of kerogen was continuously expanded and extended forward, as shown in Figure 3. From the second year, a large quantity of kerogen near profile II began to pyrolyze and more pyrolysis hydrocarbon products were generated. Therefore, the green and red lines in Figure 5b showed higher IC_2, IC_{13}, and IC_{37} contents and the closer to the production well, the lower the IC_2 and IC_{13} contents. Due to the further cracking of heavy oil at high temperature, the IC_{37} content change curves of the second and third years of in situ conversion show different laws, and there is a content peak between the heater and the producer. In addition, the hydrocarbon products produced by the cracking of organic matter near profile II will diffuse in the direction of low concentration and low pressure. This explains the fact that profile I shows that hydrocarbon products still exist in the range of a dimensionless distance of 0.44 rather than a farther distance at in situ conversion for 3 years.

The average reservoir temperature and pyrolysis hydrocarbon production of organic-rich shale in situ conversion via Sc-CO_2 for the simulation model are shown in Figure 6. With supercritical CO_2 injection, the reservoir temperature rises

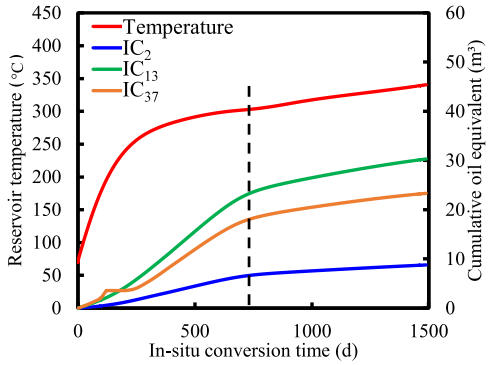

Figure 6. Changes of the reservoir temperature and hydrocarbon production.

rapidly, and IC_2, IC_{13}, and IC_{37} generated are developed at a high rate. After shale in situ conversion for about 2 years, the average reservoir temperature reaches 300 °C and the cumulative pyrolysis oil and gas production curve is obviously slowed down. It is consistent with the previous findings, i.e., the organic matter pyrolysis and hydrocarbon production mainly occur in the first 2 years of in situ conversion.

4.2. Development of the ANN-Based Prediction Model. Based on the simulation model of Sc-CO_2-assisted shale in situ conversion, the reservoir temperature and cumulative equivalent oil production data obtained under different influencing factors constitute the basic database. Based on eq 4, the Pearson correlation coefficient matrix map between input factors was drawn using MATLAB, as shown in Figure 7. Because the initial temperature and pressure are functions of the formation depth, there is a complete linear correlation between the reservoir depth, temperature, and pressure. The correlation coefficients of the three are all 1, while the correlation coefficients between other factors do not

https://doi.org/10.1021/acsomega.4c00323
ACS Omega 2024, 9, 15511−15526

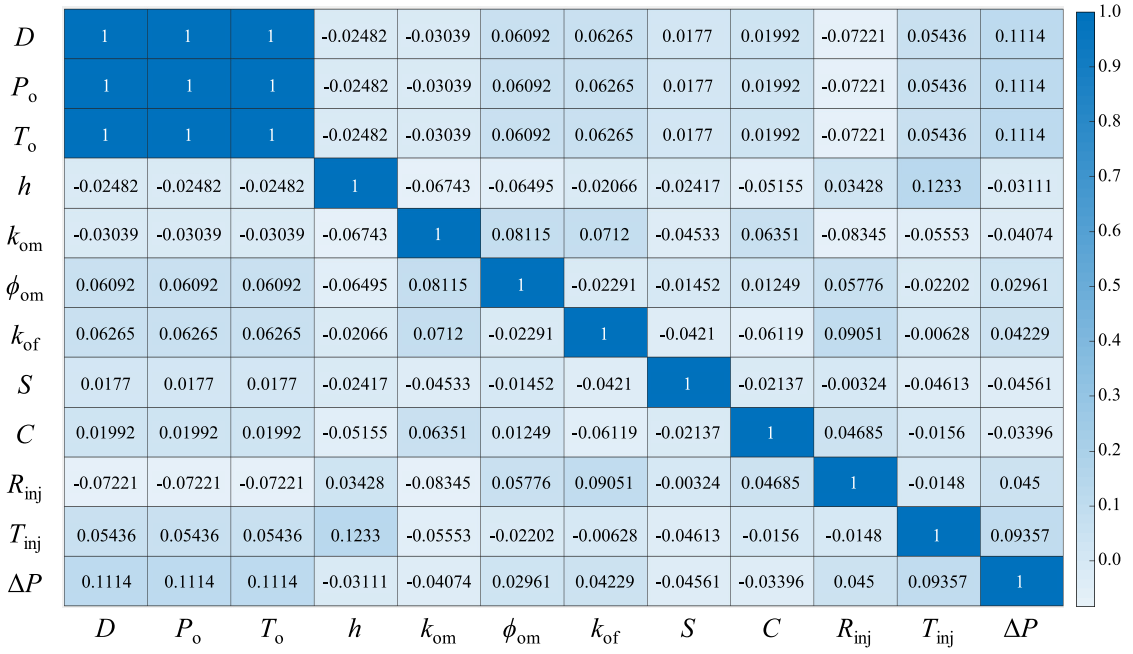

Figure 7. Diagram of the Pearson correlation coefficient matrix for input features.

show a strong correlation. Therefore, the reservoir temperature and pressure factors were removed while the remaining features were retained.

The random forest was used to determine the importance of each feature to the target response. The Gini index was used as the criterion for the training and prediction of the random forest model, and the hyperparameters were optimized, including the number of decision trees, the maximum tree depth, the minimum number of leaves, and the maximum number of features. Finally, the hyperparameters of random forest models for reservoir temperature and cumulative hydrocarbon production were determined using MATLAB, as shown in Table 4. The ranking results for the importance of the feature factors are shown in Figure 8. By setting the threshold value to 0.075,[28] the main controlling factors of objective functions were screened out and summarized, as shown in Table 5. The screened factors influencing the reservoir temperature include matrix permeability, formation depth, natural fracture permeability, Sc-CO_2 injection rate, initial kerogen concentration, Sc-CO_2 injection temperature, and thickness. The main controlling factors for hydrocarbon production are heating fluid injection rate, thickness, Sc-CO_2 injection temperature, depth, matrix and natural fracture permeability, and initial kerogen concentration.

Table 4. Performance and Hyperparameters of the Random Forest Models Constructed

	objective function	
parameters	reservoir temperature	cumulative hydrocarbon production
n_estimators	2000	1000
Max_depth	9	8
Max_feasures	4	6
Min_samples_leaf	1	1
Min_samples_split	2	2
R^2_train	1.000	0.998
R^2_test	0.937	0.953

Based on the elimination of redundant features and the screening of main features, the final sample database was determined for neural network training. Before constructing the neural network model, the data was first normalized to eliminate the influence of data scale.[29,33,54,66,67] 80% of the data was randomly selected from the optimized database to form a training set for the development of neural networks, and 20% was used for testing purposes to evaluate the prediction performance of the neural network.[67] In the network training process, the hidden layer used the hyperbolic tangent S-type transfer function (tansig) and the output layer used the linear activation function.[68] The minimum error of the training target was set to 10^{-3}, and the mean squared error was selected as the network training loss function, which could be calculated using eq 10.[61,67,68] Under different hyperparameters, the prediction accuracy of the trained neural network model is different. Therefore, it is necessary to establish multiple neural network structures and repeat the network training. The neural network has a variety of training functions that can be applied, including trainbr, trainlm, trainrp, traingdm, and traingda.[69] Different training functions were tried in turn, and the most suitable training function was determined according to the minimum MSE and the maximum determination coefficient (R^2). R^2 was used to evaluate the matching degree between the predicted value and the expected output value, which could be calculated using eq 11.[68] Finally, it is determined that the two prediction models could obtain the best results using trainbr function. The detailed structure of the BP neural network is shown in Figure 9. The optimal hyperparameter combinations with high training and prediction accuracy are listed in Table 6.

$$\mathrm{MSE} = \frac{1}{n}\sum_{i=1}^{n}(Y_{i,\mathrm{sim}} - Y_{i,\mathrm{pred}})^2 \tag{10}$$

https://doi.org/10.1021/acsomega.4c00323
ACS Omega 2024, 9, 15511−15526

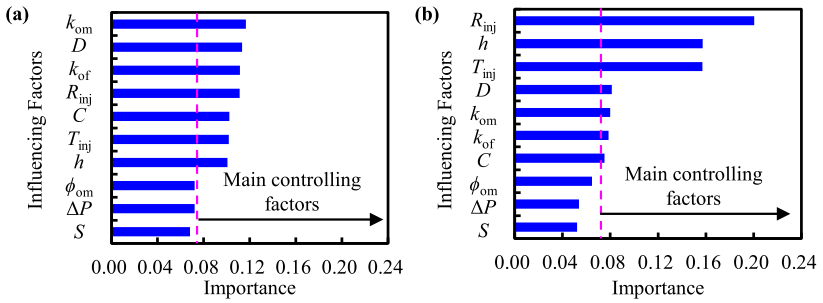

Figure 8. Ranking of feature importance determined by random forest for (a) reservoir temperature and (b) cumulative hydrocarbon production.

Table 5. Summary of the Main Controlling Factors of the Prediction Models

	objective function	
parameters	reservoir temperature	cumulative hydrocarbon production
depth (D)	√	√
thickness (h)	√	√
original permeability for matrix (k_{om})	√	√
original porosity for matrix (ϕ_{om})	×	×
original permeability for natural fracture (k_{of})	√	√
natural fracture spacing (S)	×	×
concentration of kerogen in the pore (C)	√	√
Sc-CO_2 injection rate (R_{inj})	√	√
injection temperature of Sc-CO_2 (T_{inj})	√	√
production pressure difference (ΔP)	×	×

$$R^2 = 1 - \frac{\sum_{i=1}^{n}(Y_{i,\mathrm{sim}} - Y_{i,\mathrm{pred}})^2}{\sum_{i=1}^{n}(Y_{i,\mathrm{sim}} - \overline{Y}_{i,\mathrm{sim}})^2} \quad (11)$$

Table 6. Optimal Hyperparameters for the ANN-Based Prediction Models

	objective function	
hyperparameter	reservoir temperature	cumulative hydrocarbon production
number of the hidden layers	2	1
number of the hidden neurons	42, 42	11
learning rate	0.03	0.03
training function	trainbr	trainbr
transfer function	tansig	tansig
training epochs	100	200

where $Y_{i,\mathrm{sim}}$, $Y_{i,\mathrm{pred}}$, and $-Y_{i,\mathrm{sim}}$ are the data from simulation results, the prediction value by the BP neural network, and the average of simulation data, respectively.

The training set error of the obtained reservoir temperature prediction model under the optimal hyperparameters is 0.12%, and the testing set error is 0.18%. The errors of the training set and testing set for the cumulative hydrocarbon expulsion prediction model are 0.17 and 0.30%, respectively. Figure 10 shows the cross plot between the simulated and predicted data for the two prediction models, in which the scatter points are distributed near the 45° line. The overall R^2 of the reservoir temperature prediction model is 97.52%, and the overall

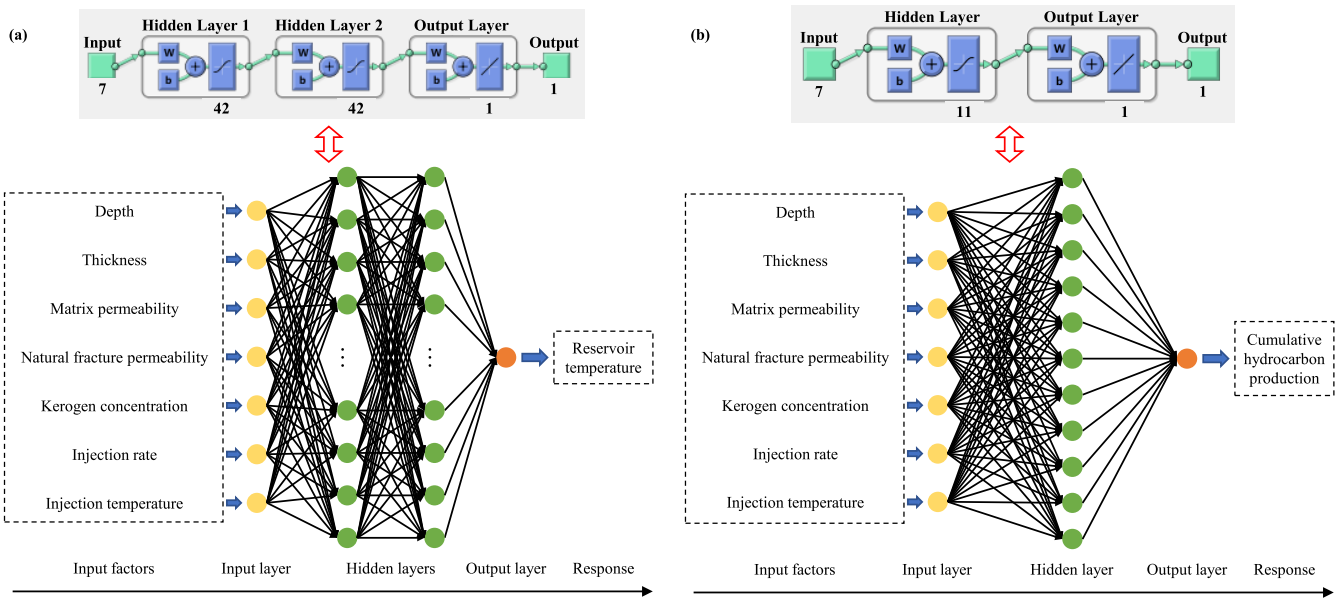

Figure 9. Structure of ANN-based prediction models for (a) reservoir temperature and (b) cumulative hydrocarbon production.

https://doi.org/10.1021/acsomega.4c00323
ACS Omega 2024, 9, 15511−15526

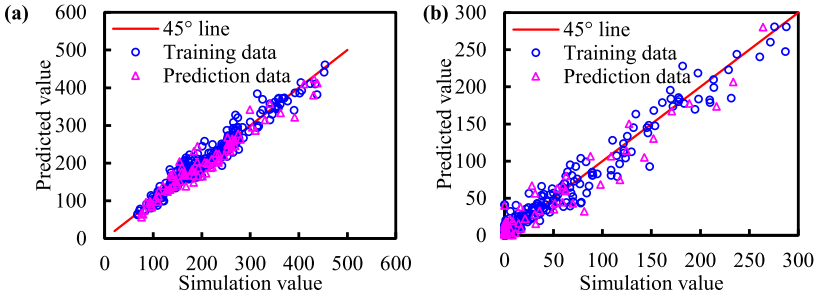

Figure 10. Cross plot of simulation data and prediction data for (a) the reservoir temperature prediction model and (b) the cumulative hydrocarbon production prediction model.

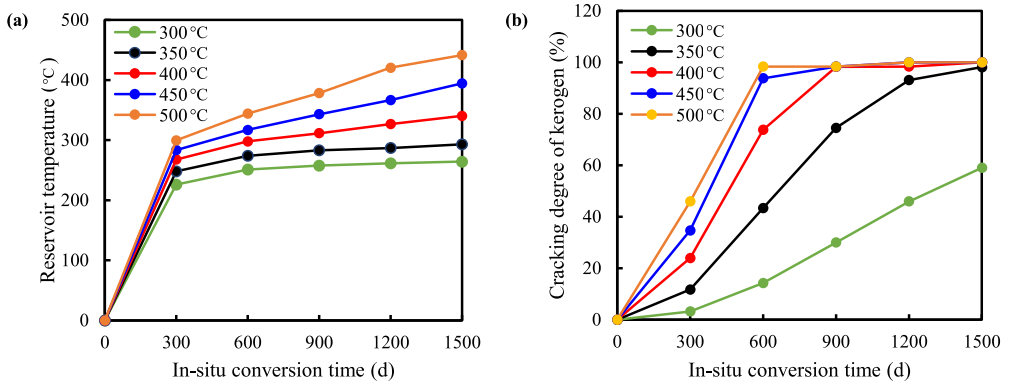

Figure 11. Effects of the injection temperature on (a) the reservoir temperature and (b) the cracking degree of kerogen.

accuracy of the cumulative hydrocarbon production prediction model is 97.28%. It is concluded that the established performance prediction model of Sc-CO_2-assisted organic-rich shale in situ conversion can accurately predict the reservoir temperature and cumulative hydrocarbon production. It helps the rapid optimization of the development design of organic-rich shale reservoirs under different working conditions.

Model verification is necessary for artificial neural network modeling. The prediction model was run to determine the reservoir temperature and cumulative hydrocarbon production of shale in situ conversion under the reservoir conditions and development parameters given in Section 2. The accuracy of established ANN-based prediction models is verified by comparing its outputs with the simulation outputs presented in Section 4.1. The reservoir temperature and cumulative hydrocarbon production obtained by the CMG-STARS module simulation were 340.43 °C and 62.394 m^3, respectively. The reservoir temperature and cumulative hydrocarbon production determined by the ANN-based prediction model were 345.78 °C and 64.078 m^3, respectively. The accuracies of the prediction models for reservoir temperature and cumulative hydrocarbon production were 98.43 and 97.30%, respectively, which fully reflected the reliability of the ANN-based prediction models established in this paper.

4.3. Sensitivity Analysis. Temperature determines the organic matter pyrolysis rate. The flow rate and pressure are key features affecting the production performance of the shale reservoir. Therefore, the sensitivity of the shale in situ conversion effect to three factors including injection temperature, injection rate, and production pressure difference was analyzed. On the one hand, the influence of factors on in situ conversion production can be clarified. On the other hand, the accuracy of prediction models in computation framework can be further verified.

4.3.1. Effect of Injection Temperature on Shale In Situ Conversion. Based on the established simulation model and prediction model, shale in situ conversion effects at injection temperatures of 300, 350, 400, 450, and 500 °C were calculated, respectively. The prediction errors for the reservoir temperature and hydrocarbon production at different injection temperatures are all within 5%, which further verifies the accuracy of the constructed prediction models. The average reservoir temperature obtained by simulation is shown in Figure 11a, and the degree of kerogen cracking at different injection temperatures was plotted, as shown in Figure 11b. With the increase in injection temperature, the reservoir temperature rises at a higher rate, the kerogen cracking process is accelerated, and the time required for kerogen complete cracking is shorter. When the injection temperature is higher than 450 °C, the complete pyrolysis of kerogen can be basically achieved at in situ conversion for 600 days.

The hydrocarbon gas, light oil, and heavy oil generated are discharged through the seepage channel. The changes in the content of hydrocarbon gas, light oil, and heavy oil produced at different injection temperatures are shown in Figure 12. With the uniform increase in injection temperature, hydrocarbon gas and light oil contents increase at a smaller and smaller rate and the content of the two change little above 450 °C. The content of heavy oil increases gradually in the range of 300−450 °C and decreases in the range of 450−500 °C, indicating that the cracking rate of heavy oil in this temperature range is higher than that of kerogen cracking.

In addition, the heat loss of the bedrock is considered to be a waste of energy and uneconomically behaves. The energy

https://doi.org/10.1021/acsomega.4c00323
ACS Omega 2024, 9, 15511−15526

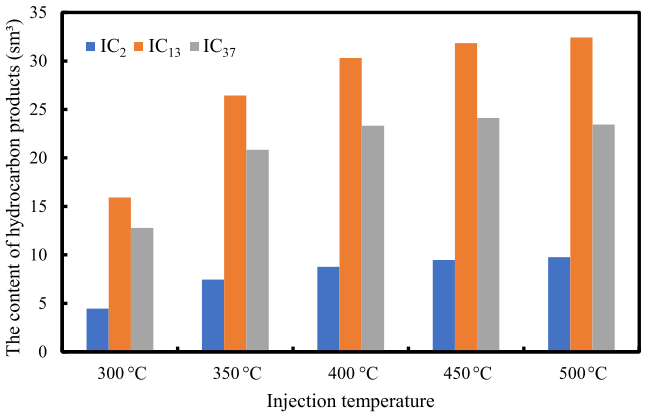

Figure 12. Contents of hydrocarbon products at different injection temperatures.

conversion ratio (ECR) is an important index to evaluate the application of shale in situ conversion technology. Therefore, the heat loss and ECR at different injection temperatures were compared, as shown in Figure 13. The ECR is defined as the ratio of the produced hydrocarbon heat energy to the injected heat energy during shale in situ conversion. The energy contained in the produced fluid is measured by the reaction heat of the cumulative hydrocarbon, and the unit oil equivalent is set to contain 40 GJ energy.[13,37,70] The injected energy is determined by the difference between the heat of injected high-temperature supercritical CO_2 and the residual heat of the produced gas.

With the continuous injection of thermal fluid, the heat loss of the bedrock is increasing. The higher the temperature of the injected fluid, the greater the final heat loss. At low injection temperatures, organic matter is pyrolyzed and hydrocarbons are continuously accumulated within 1500 days of shale in situ conversion. The ECR gradually increases with time. At high injection temperatures, most of the kerogen is rapidly pyrolyzed in the early stage and only a small amount of kerogen is pyrolyzed in the later stage, as shown in Figure 11b. Therefore, the ECR increases first and then decreases. Moreover, the peak of the ECR appears earlier with an increase in injection temperature. This means that the higher the injection temperature, the less shale in situ conversion time is needed to maximize energy utilization. Considering that organic matter cracking and hydrocarbon product discharge mainly occur in the first 2 years of in situ conversion exploitation, the optimal injection temperature for different in situ conversion periods is given in Figure 13b. In the early stage of shale in situ conversion development, a high injection temperature allows more organic matter to be cracked and a higher ECR can be obtained. In the later stage of shale in situ conversion development, the remaining organic matter in the reservoir at high injection temperatures is not much and the energy generated by organic matter cracking is not enough to make up for the energy consumption of the injected heating fluid. Therefore, with the extension of the in situ conversion time, the temperature required to achieve the maximum ECR is lower. After shale in situ conversion for 1200 days, the optimal injection temperature is maintained at 350 °C. Therefore, considering in situ conversion hydrocarbon expulsion production and energy utilization, the reservoir can choose to inject 350−450 °C thermal fluid to obtain a more promising mining effect.

4.3.2. Effect of Injection Rate on Shale In Situ Conversion. The numerical simulation of in situ conversion with injection rates of 200, 400, 600, 800, and 1000 m^3/day was carried out. Shale reservoir temperature and the characteristics of hydrocarbon products at different injection rates are shown in Figure 14. With the increase in the Sc-CO_2 injection rate, the reservoir temperature rises faster, the time for kerogen to start cracking is shorter, and more kerogen participates in the reaction, accompanied by more pyrolysis hydrocarbon generation. The pyrolysis hydrocarbon products gradually migrate to production driven and carried by supercritical CO_2 fluid. Therefore, with the increase in Sc-CO_2 injection rate, oil and gas production increased rapidly, as shown in Figure 14b. However, when the injection rate is higher than 600 m^3/day, the heating effect of thermal fluid on the shale reservoir does not produce a greater temperature enhance. At the same time, the yield change curves of IC_2, IC_{13}, and IC_{37} slowed down.

Supercritical fluids are continuously injected into the reservoir and gradually spread to production wells. It continuously heats the rock, and solid kerogen begins to crack to generate hydrocarbons. Under continuous drive of Sc-CO_2 fluid, formation water, and pyrolysis gas, the pyrolysis hydrocarbon products are discharged from the generated pores. This process has largely caused increases in reservoir porosity and permeability. Therefore, the variation curves of porosity and permeability of typical grid unit {13,13,2} during shale in situ conversion are drawn, as shown in Figure 15.

As the injection rate of supercritical fluid increases, the kerogen of the grid cell pyrolyzes earlier and the porosity and permeability begin to increase earlier. When the injection rate is 200 m^3/day, the reservoir temperature rises to 250 °C within

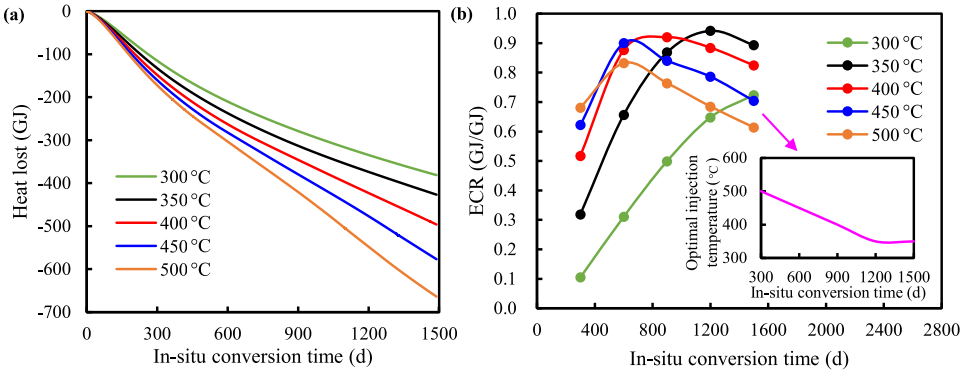

Figure 13. Energy utilization performance at different injection temperatures: (a) reservoir heat lost and (b) energy conversion ratio.

https://doi.org/10.1021/acsomega.4c00323
ACS Omega 2024, 9, 15511−15526

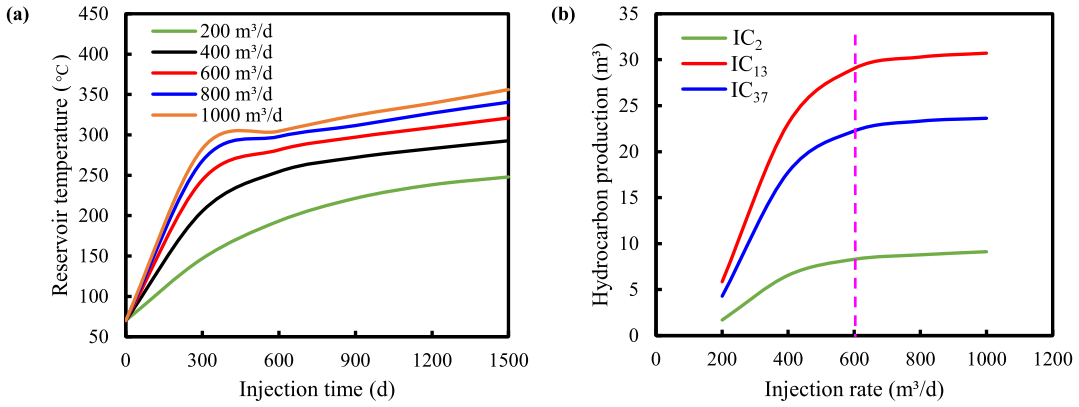

Figure 14. Effect of the injection rates on (a) reservoir temperature and (b) hydrocarbon production.

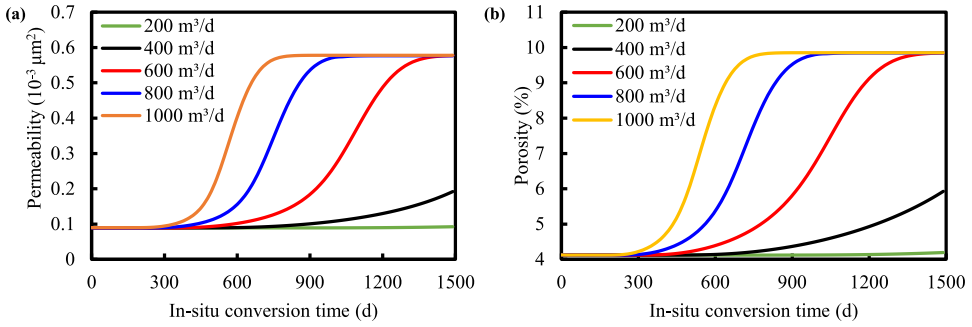

Figure 15. Effect of the injection rates on (a) permeability and (b) porosity.

1500 days of the operation time, which has not yet reached the temperature range of effective kerogen pyrolysis and the grid has only 1.27% of kerogen pyrolysis. When the injection rate is 400 m^3/day, only 31.4% of the kerogen is cracked, the porosity is 1.43 times higher than that of the original, and the permeability is 2.14 times higher. The low injection fluid rate leads to a significant extension of the effective development period of shale in situ conversion. For an injection rate higher than 600 m^3/day, the kerogen of the grid cell is basically completely pyrolyzed, the porosity is up to 2.39 times, and the permeability is up to 6.44 times. It can be concluded that the injection rate of 600 m^3/day has been able to meet the needs of shale in situ conversion development.

4.3.3. Effect of Production Pressure on Shale In Situ Conversion. The numerical simulation of in situ conversion with production pressure differences of 2, 4, and 6 MPa was performed, and the results are drawn in Figure 16. In the case of sufficient supercritical fluid injection, the carrying and gas driving mechanisms make the generated pyrolysis oil and gas discharge, which depends on a small extent on the production pressure difference. There is no difference in reservoir temperature or pyrolysis hydrocarbon yield under various production pressure differences. Therefore, for shale in situ conversion by supercritical fluid heating, the production pressure difference has little effect on the development performance, which is consistent with the main controlling factors screened based on random forest.

4.4. Operation Optimization. The maximum hydrocarbon production obtained by shale in situ conversion is often the most concerning to researchers. Therefore, the ANN-based prediction model of cumulative hydrocarbon production established in Section 4.2 is used as the proxy model. The PSO algorithm is adopted to optimize heating parameters,

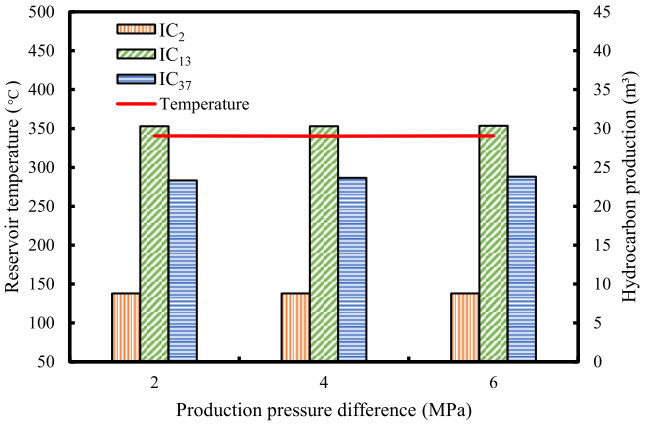

Figure 16. Effect of the production pressure difference on the shale in situ conversion performance.

including injection rate, and injection temperature, so the framework can avoid a lot of numerical calculations. In this paper, according to the characteristics of continental organic-rich shale reservoirs, three typical reservoir characteristic types are considered, which represent the organic-rich shale layers of Ordos Basin, Songliao Basin, and Junggar Basin, respectively.[1−4] The development parameter optimization under specific reservoir properties is performed. Considering that the optimization algorithm may obtain different optimization performances in each calculation, multiple PSO optimization calculations for each typical case were carried out. The convergence curve of cumulative hydrocarbon production is shown in Figure 17. Typical reservoir properties and determined optimal development parameters are listed in Table 7.

https://doi.org/10.1021/acsomega.4c00323
ACS Omega 2024, 9, 15511−15526

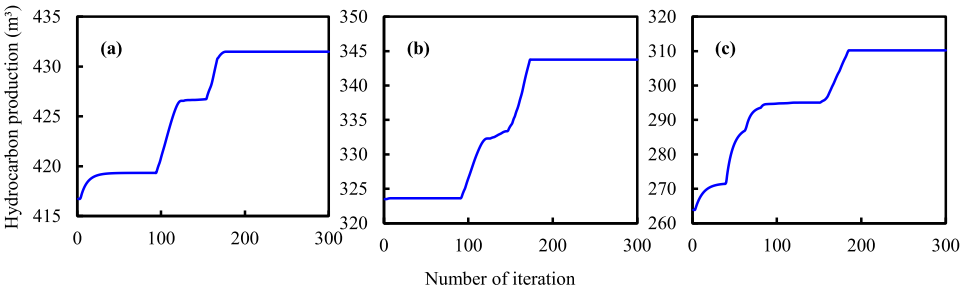

Figure 17. Convergence curve of cumulative hydrocarbon production for (a) case 1, (b) case 2, and (c) case 3.

Table 7. PSO-Based Optimization Results of Typical Cases

	depth (m)	thickness (m)	original permeability for matrix (10^{-3} μm^2)	original permeability for natural fracture (10^{-3} μm^2)	concentration of kerogen in the pore (mol/m^3)	optimal injection rate	optimal injection temperature
case 1	1000	60	0.1	50	20,000	1000	521.05
case 2	2000	90	0.15	100	5000	1000	510.55
case 3	3000	120	0.05	10	10,000	1000	507.44

We have applied cases of typical reservoir properties to optimize the corresponding development parameters. However, a large number of numerical simulations are carried out with fixed heating fluids and well patterns to construct the database, which makes the application of the current in situ conversion performance prediction and optimization model have certain limitations. Therefore, in future research, the shale in situ conversion development with different heating fluids and well patterns should be taken as the direction, supplemented by the field data of shale in situ conversion, to further enrich the sample database and expand the prediction and optimization model.

5. CONCLUSIONS

The numerical simulation of shale in situ conversion via Sc-CO_2 injection was carried out, and the characteristics of organic matter conversion, fluid distribution, and generated product release were analyzed. A database was constructed, and rapid prediction models for reservoir temperature and cumulative hydrocarbon production based on ANN were obtained. The sensitivity analysis of shale in situ conversion development performance was conducted, which not only clarified the development laws under different heating parameters but also further verified the ANN prediction models. The PSO algorithm was performed to optimize heating parameters using the ANN prediction model as a proxy. The following conclusions can be drawn:

1. Kerogen cracking and hydrocarbon product discharge mainly occurred in the first 2 years of shale in situ conversion, when the reservoir temperature reached 300 °C, with an average of 82.5% of kerogen pyrolysis. After that, the production curves of hydrocarbon gas, light oil, and heavy oil slowed down significantly.
2. A database with 430 numerical simulation data was constructed. Pearson correlation analysis and random forest method were applied to optimize the database, and seven main controlling factors affecting reservoir temperature and hydrocarbon production were screened out.
3. The proposed ANN-based prediction models can achieve high-precision predictions for reservoir temperature and hydrocarbon production. Under the optimal neural network structure, the determination coefficients of the prediction models for reservoir temperature and cumulative hydrocarbon production are 97.52 and 97.28%, respectively, and the MSE of both prediction models is lower than 0.3%.
4. Considering the shale in situ conversion hydrocarbon expulsion production and energy conversion characteristics, the reservoir can choose to inject 350−450 °C thermal fluid with a rate of 600 m^3/day to obtain a more promising development effect.
5. The heating parameter optimization for three typical reservoir characteristic cases was performed, and the reasonable injection temperature and injection rate were obtained, which could help engineers to rapidly design the heating schemes.

AUTHOR INFORMATION

Corresponding Author

Chuanjin Yao − *National Key Laboratory of Deep Oil and Gas, China University of Petroleum (East China), Qingdao, Shandong 266580, China; Key Laboratory of Unconventional Oil & Gas Development, China University of Petroleum (East China), Ministry of Education, Qingdao, Shandong 266580, China; School of Petroleum Engineering, China University of Petroleum (East China), Qingdao, Shandong 266580, China;* orcid.org/0000-0002-6125-8991; Email: cy375@upc.edu.cn

Authors

Yaqian Liu − *National Key Laboratory of Deep Oil and Gas, China University of Petroleum (East China), Qingdao, Shandong 266580, China; Key Laboratory of Unconventional Oil & Gas Development, China University of Petroleum (East China), Ministry of Education, Qingdao, Shandong 266580, China; School of Petroleum Engineering, China University of Petroleum (East China), Qingdao, Shandong 266580, China*

Baishuo Liu − *National Key Laboratory of Deep Oil and Gas, China University of Petroleum (East China), Qingdao, Shandong 266580, China; Key Laboratory of Unconventional Oil & Gas Development, China University of Petroleum (East China), Ministry of Education, Qingdao, Shandong 266580, China; School of Petroleum Engineering,*

https://doi.org/10.1021/acsomega.4c00323
ACS Omega 2024, 9, 15511−15526

China University of Petroleum (East China), Qingdao, Shandong 266580, China

Yangyang Xuan − *National Key Laboratory of Deep Oil and Gas, China University of Petroleum (East China), Qingdao, Shandong 266580, China; Key Laboratory of Unconventional Oil & Gas Development, China University of Petroleum (East China), Ministry of Education, Qingdao, Shandong 266580, China; School of Petroleum Engineering, China University of Petroleum (East China), Qingdao, Shandong 266580, China*

Xinge Du − *National Key Laboratory of Deep Oil and Gas, China University of Petroleum (East China), Qingdao, Shandong 266580, China; Key Laboratory of Unconventional Oil & Gas Development, China University of Petroleum (East China), Ministry of Education, Qingdao, Shandong 266580, China; School of Petroleum Engineering, China University of Petroleum (East China), Qingdao, Shandong 266580, China*

Complete contact information is available at: https://pubs.acs.org/10.1021/acsomega.4c00323

Notes

The authors declare no competing financial interest.

■ ACKNOWLEDGMENTS

This research was supported by the National Natural Science Foundation of China (Grant Nos. U22B6004, 51974341), the Fundamental Research Funds for the Central Universities (No. 20CX06070A), and the Science and Technology Support Plan for Youth Innovation of University in Shandong Province (Grant No. 2019KJH002). We also appreciate the reviewers and editors for their constructive comments to make the paper high quality.

■ NOMENCLATURE

Sc-CO_2 supercritical CO_2
ANN artificial neural network
BP back-propagation
VIM variation importance measures
D reservoir depth
h reservoir thickness
P_0 original reservoir pressure
T_0 original reservoir temperature
k_{om} original permeability for matrix
ϕ_{om} original porosity for matrix
k_{of} original permeability for natural fracture
S natural fracture spacing
C concentration of kerogen in the pore
R_{inj} heating fluid injection rate
T_{inj} heating fluid injection temperature
ΔP Production pressure difference
MSE mean square error
R^2 determination coefficient

■ REFERENCES

(1) Zhao, W.; Hu, S.; Hou, L. Connotation and strategic role of in-situ conversion processing of shale oil underground in the onshore China. *Petrol. Explor. Dev.* **2018**, *45* (4), 563−572.

(2) ZHAO, W.; HU, S.; HOU, L.; YANG, T.; LI, X.; GUO, B.; YANG, Z.; et al. Types and resource potential of continental shale oil in China and its boundary with tight oil. *Pet. Explor. Dev.* **2020**, *47* (1), 1−11.

(3) Zou, C.; Pan, S.; Jing, Z.; et al. Shale oil and gas revolution and its impact. *Acta Pet. Sin.* **2020**, *41* (1), 1.

(4) Wang, S.; Jiang, X.; Han, X.; et al. Investigation of Chinese oil shale resources comprehensive utilization performance. *Energy* **2012**, *42* (1), 224−232.

(5) Han, X.; Niu, M.; Jiang, X. Combined fluidized bed retorting and circulating fluidized bed combustion system of oil shale: 2. Energy and economic analysis. *Energy* **2014**, *74*, 788−794.

(6) Kang, Z.; Zhao, Y.; Yang, D. Review of oil shale in-situ conversion technology. *Appl. Energy* **2020**, *269*, No. 115121.

(7) Raukas, A.; Punning, J.-M. Environmental problems in the Estonian oil shale industry. *Energy Environ. Sci.* **2009**, *2*, 723−8.

(8) Crawford, P. M.; Killen, J. C. New challenges and directions in oil shale development technologies. *Oil shale: A solution to the liquid fuel dilemma: ACS Publications* **2010**, *1032*, 21−60.

(9) Lin, L.; Lai, D.; Guo, E.; et al. Oil shale pyrolysis in indirectly heated fixed bed with metallic plates of heating enhancement. *Fuel* **2016**, *163*, 48−55.

(10) HAO, Y.; XIAOQIAO, G.; FANSHENG, X.; JIALIANG, Z.; YANJU, L.; et al. Temperature distribution simulation and optimization design of electric heater for in-situ oil shale heating. *Oil Shale* **2014**, *31*, 105−20.

(11) Wang, L.; Yang, D.; Kang, Z. Evolution of permeability and mesostructure of oil shale exposed to high-temperature water vapor. *Fuel* **2021**, *290*, No. 119786.

(12) Kang, Z.; Zhao, Y.; Yang, D.; et al. A pilot investigation of pyrolysis from oil and gas extraction from oil shale by in-situ superheated steam injection. *J. Petrol. Sci. Eng.* **2020**, *186*, No. 106785.

(13) Pei, S.; Wang, Y.; Zhang, L.; et al. An innovative nitrogen injection assisted in-situ conversion process for oil shale recovery: Mechanism and reservoir simulation study. *J. Petrol. Sci. Eng.* **2018**, *171*, 507−515.

(14) Allawzi, M.; Al-Otoom, A.; Allaboun, H.; et al. CO_2 supercritical fluid extraction of Jordanian oil shale utilizing different co-solvents. *Fuel Process. Technol.* **2011**, *92* (10), 2016−2023.

(15) Liang, X.; Zhao, Q.; Dong, Y.; et al. Experimental investigation on supercritical water gasification of organic-rich shale with low maturity for syngas production. *Energy Fuels* **2021**, *35* (9), 7657−7665.

(16) Yu, C.; Zhao, X.; Jiang, Q.; et al. Shale Microstructure Characteristics under the Action of Supercritical Carbon Dioxide (Sc-CO_2). *Energies* **2022**, *15* (22), 8354.

(17) Wu, T.; Xue, Q.; Li, X.; et al. Extraction of kerogen from oil shale with supercritical carbon dioxide: Molecular dynamics simulations. *Journal of Supercritical Fluids* **2016**, *107*, 499−506.

(18) Mozaffari, S.; Järvik, O.; Baird, Z. S. Effect of N_2 and CO_2 on shale oil from pyrolysis of Estonian oil shale. *International Journal of Coal Preparation and Utilization* **2022**, *42* (10), 2908−2922.

(19) Shuai, Z.; Xiaoshu, L.; Qiang, L.; Youhong, S.; et al. Thermal-fluid coupling analysis of oil shale pyrolysis and displacement by heat-carrying supercritical carbon dioxide. *Chem. Eng. J.* **2020**, *394*, No. 125037.

(20) Lee, K.; Moridis, G. J.; Ehlig-Economides, C. A.Oil shale in-situ upgrading by steam flowing in vertical hydraulic fractures. *SPE Unconventional Resources Conference/Gas Technology Symposium*; SPE 2014, D011S002R001.

(21) Lee, K.; Moridis, G. J.; Ehlig-Economides, C. A. A comprehensive simulation model of kerogen pyrolysis for the in-situ upgrading of oil shales. *SPE J.* **2016**, *21* (05), 1612−1630.

(22) Shen, C. Reservoir simulation study of an in-situ conversion pilot of Green-River oil shale. *SPE Rocky Mountain Petroleum Technology Conference/Low-Permeability Reservoirs Symposium* SPE 2009, SPE-123142-MS. DOI: 10.2118/123142-MS.

(23) Zhu, C.; Guo, W.; Sun, Y.; et al. Reaction mechanism and reservoir simulation study of the high-temperature nitrogen injection in-situ oil shale process: A case study in Songliao Basin, China. *Fuel* **2022**, *316*, No. 123164.

(24) Youtsos, M-S-K.; Mastorakos, E.; Cant, R. S. Numerical simulation of thermal and reaction fronts for oil shale upgrading. *Chemi. Eng. Sci.* **2013**, *94*, 200−213.
(25) Zhao, J.; Wang, L.; Liu, S.; et al. Numerical simulation and thermo-hydro-mechanical coupling model of in situ mining of low-mature organic-rich shale by convection heating. *Advances in Geo-Energy Research* **2022**, *6* (6), 502−514.
(26) Wang, Z.; Yao, J.; Sun, H.; et al. Numerical simulation of thermal-reactive flow coupling during the in-situ conversion of medium to low maturity shale reservoirs. *Acta Pet. Sin.* **2022**, *43* (10), 1462.
(27) Zhou, G.; Guo, Z.; Sun, S.; et al. A CNN-BiGRU-AM neural network for AI applications in shale oil production prediction. *Applied Energy* **2023**, *344*, No. 121249.
(28) Huang, S.; Tian, L.; Zhang, J.; et al. Support Vector Regression Based on the Particle Swarm Optimization Algorithm for Tight Oil Recovery Prediction. *ACS omega* **2021**, *6* (47), 32142−32150.
(29) Luo, S.; Ding, C.; Cheng, H.; et al. Estimated ultimate recovery prediction of fractured horizontal wells in tight oil reservoirs based on deep neural networks. *Advances in Geo-Energy Research* **2022**, *6* (2), 111−122.
(30) Vo Thanh, H.; Sugai, Y.; Sasaki, K. Application of artificial neural network for predicting the performance of CO_2 enhanced oil recovery and storage in residual oil zones. *Sci. Rep.* **2020**, *10* (1), 18204.
(31) Chahar, J.; Verma, J.; Vyas, D.; et al. Data-driven approach for hydrocarbon production forecasting using machine learning techniques. *J. Petrol. Sci. Eng.* **2022**, *217*, No. 110757.
(32) Ebrahimi, A.; Khamehchi, E. Developing a novel workflow for natural gas lift optimization using advanced support vector machine. *J. Natural Gas Sci. Eng.* **2016**, *28*, 626−638.
(33) Chen, H.; Wang, Y.; Zuo, M.; et al. A new prediction model of CO_2 diffusion coefficient in crude oil under reservoir conditions based on BP neural network. *Energy* **2022**, *239*, No. 122286.
(34) Al-Khafaji, F. H.; Meng, Q.; Hussain, W.; Khudhair Mohammed, R.; Harash, F.; Alshareef AlFakey, S.; et al. Predicting minimum miscible pressure in pure CO_2 flooding using machine learning: Method comparison and sensitivity analysis. *Fuel* **2023**, *354*, No. 129263.
(35) Kalam, S.; Yousuf, U.; Abu-Khamsin, S. A.; et al. An ANN model to predict oil recovery from a 5-spot waterflood of a heterogeneous reservoir. *J. Petrol. Sci. Eng.* **2022**, *210*, No. 110012.
(36) You, J.; Ampomah, W.; Kutsienyo, E J. Assessment of enhanced oil recovery and CO_2 storage capacity using machine learning and optimization framework. *SPE Europec featured at EAGE Conference and Exhibition*; SPE 2019, D041S008R006. DOI: 10.2118/195490-MS.
(37) Fan, Y.; Durlofsky, J.; Tchelepi, H. Numerical simulation of the in-situ upgrading of oil shale. *SPE J.* **2010**, *15*, 368−381.
(38) Fowler, T. D.; Vinegar, H. J. Oil shale ICP-Colorado field pilots. *SPE western regional meeting*; OnePetro, 2009. DOI: 10.2118/121164-MS.
(39) Kang, Z.; Zhao, Y.; Yang, D. Physical principle and numerical analysis of oil shale development using in-situ conversion process technology. *Acta Pet. Sin.* **2008**, *29* (4), 592.
(40) Li, Y.; Xue, L.; Ma, J. Numerical simulation of the changes of porosity and permeability in in-situ pyrolysis of oil shale. *Sci. Technol. Eng.* **2018**, *18* (34), 43−50.
(41) Ma, Y.; Li, S. The mechanism and kinetics of oil shale pyrolysis in the presence of water. *Carbon Resources Conversion* **2018**, *1* (2), 160−4.
(42) Fucinos, R.; Voskov, D.; Burnham, A. K. Hierarchical coarsening of simulation model for in-situ upgrading process. *SPE Reservoir Simulation Conference*; SPE 2017. DOI: 10.2118/182675-MS.
(43) Braun, R. L.; Burnham, A. K. Pmod: a flexible model of oil and gas generation, cracking, and expulsion. *Org. Geochem.* **1992**, *19*, 161−172.
(44) Wellington, S. L.et al.*In Situ thermal Processing of an Oil Shale Formation to Produce a Condensate*. 2005. (Google Patents).
(45) Lee, K. J.; Finsterle, S.; Moridis, G. J. Analyzing the impact of reaction models on the production of hydrocarbons from thermally upgraded oil shales. *J. Petrol. Sci. Eng.* **2018**, *168*, 448−64.
(46) Lei, G.; Li, Z.; Yao, C.; et al. Numerical simulation on in-situ upgrading of oil shale via steam injection. *J. Univ. Pet. China* **2017**, *41*, 100−107.
(47) Braun, R. L.; Burnham, A. K. Mathematical model of oil generation, degradation, and expulsion. *Energy Fuels* **1990**, *4* (2), 132−46.
(48) Pei, S.; Cui, G.; Wang, Y.; et al. Air assisted in situ upgrading via underground heating for ultra heavy oil: Experimental and numerical simulation study. *Fuel* **2020**, *279*, No. 118452.
(49) Jin, Z.; Wang, G.; Liu, G.; et al. Research progress and key scientific issues of continental shale oil in China. *Acta Pet. Sin.* **2021**, *42* (7), 821.
(50) Du, J.; Hu, S.; Pang, Z.; et al. The types, potentials and prospects of continental shale oil in China. *Chin. Pet. Explor.* **2019**, *24* (5), 560.
(51) Nguyen-Le, V.; Shin, H. Artificial neural network prediction models for Montney shale gas production profile based on reservoir and fracture network parameters. *Energy* **2022**, *244*, No. 123150.
(52) Pearson, K. VII Mathematical contributions to the theory of evolution.—III. Regression, heredity, and panmixia. *Philosophical Transactions of the Royal Society of London Series A, containing papers of a mathematical or physical character* **1896**, *187*, 253−318, DOI: 10.1098/rsta.1896.0007.
(53) Niu, W.; Lu, J.; Sun, Y. A production prediction method for shale gas wells based on multiple regression. *Energies* **2021**, *14* (5), 1461.
(54) Zhang, R.; Jia, H. Production performance forecasting method based on multivariate time series and vector autoregressive machine learning model for waterflooding reservoirs. *Petrol. Explor. Dev.* **2021**, *48* (1), 201−211.
(55) Breiman, L. Random forests. *Machine Learning* **2001**, *45*, 5−32.
(56) Jiang, F.; Huo, L.; Chen, D.; et al. The controlling factors and prediction model of pore structure in global shale sediments based on random forest machine learning. *Earth-Science Reviews* **2023**, *241*, No. 104442.
(57) Bhattacharya, S.; Mishra, S. Applications of machine learning for facies and fracture prediction using Bayesian Network Theory and Random Forest: Case studies from the Appalachian basin, USA. *J. Petrol. Sci. Eng.* **2018**, *170*, 1005−1017.
(58) Hornik, K.; Stinchcombe, M.; White, H. Multilayer feedforward networks are universal approximators. *Neural Network* **1989**, *2* (5), 359.
(59) Mittal, S.; Pathak, S.; Dhawan, H.; Upadhyayula, S. A machine learning approach to improve ignition properties of high-ash Indian coals by solvent extraction and coal blending. *Chem. Eng. J.* **2021**, *413*, No. 127385.
(60) Cheng, J.; Wang, X.; Si, T.; Zhou, F.; Zhou, J.; Cen, K.; et al. Ignition temperature and activation energy of power coal blends predicted with back-propagation neural network models. *Fuel* **2016**, *173*, 230.
(61) Ahmadi, M. A. Neural network based unified particle swarm optimization for prediction of asphaltene precipitation. *Fluid Phase Equilib.* **2012**, *314*, 46−51.
(62) Eberhart, R.; Kennedy, J. A new optimizer using particle swarm theory. *Proceedings of the sixth international symposium on micro machine and human science*; IEEE 1995, 39−43. DOI: 10.1109/MHS.1995.494215.
(63) Karkevandi-Talkhooncheh, A.; Hajirezaie, S.; Hemmati-Sarapardeh, A.; et al. Application of adaptive neuro fuzzy interface system optimized with evolutionary algorithms for modeling CO_2-crude oil minimum miscibility pressure. *Fuel* **2017**, *205*, 34−45.
(64) Lu, C.; Jiang, H.; Yang, J.; et al. Shale oil production prediction and fracturing optimization based on machine learning. *J. Petrol. Sci. Eng.* **2022**, *217*, No. 110900.

https://doi.org/10.1021/acsomega.4c00323
ACS Omega 2024, 9, 15511−15526

(65) Onwunalu, J. E.; Durlofsky, L. J. Application of a particle swarm optimization algorithm for determining optimum well location and type. *Comput. Geosci* **2010**, *14*, 183−198.
(66) Choubineh, A.; Helalizadeh, A.; Wood, D. A. Estimation of minimum miscibility pressure of varied gas compositions and reservoir crude oil over a wide range of conditions using an artificial neural network model. *Advances in Geo-Energy Research* **2019**, *3* (1), 52−66.
(67) Alwated, B.; El-Amin, M. F. Enhanced oil recovery by nanoparticles flooding: From numerical modeling improvement to machine learning prediction. *Advances in Geo-Energy Research* **2021**, *5* (3), 297−317.
(68) Yadav, A. M.; Chaurasia, R. C.; Suresh, N.; et al. Application of artificial neural networks and response surface methodology approaches for the prediction of oil agglomeration process. *Fuel* **2018**, *220*, 826−836.
(69) Liang, W.; Wang, G.; Ning, X.; et al. Application of BP neural network to the prediction of coal ash melting characteristic temperature. *Fuel* **2020**, *260*, No. 116324.
(70) Yang, L.; Zhu, C.; Zeng, H.; et al. Numerical simulation analysis on the development effect of vertical well and horizontal well during oil shale autothermic pyrolysis in-situ conversion process: a case study of oil shale in Xunyi area, Ordos Basin. *Acta Pet. Sin.* **2023**, *44* (8), 1333.

https://doi.org/10.1021/acsomega.4c00323
ACS Omega 2024, 9, 15511−15526